



Surface roughness optimization of hybrid PBF-LB/M-built Inconel 718 using in situ high-speed milling

David Sommer¹ · Simon Hornung¹ · Cemal Esen² · Ralf Hellmann¹

Received: 25 August 2023 / Accepted: 1 March 2024 / Published online: 23 March 2024
© The Author(s) 2024

Abstract

We report on the optimization of the surface roughness of hybrid additive manufactured Ni superalloys, combining a conventional laser powder bed fusion process with in situ high-speed milling. This remarkable hybrid approach has only recently been applied to different steel types and barely to Ni superalloys which opposite to steel appear to be challenging for milling processes, particularly within the powderbed of laser powder bed fusion. Different influencing factors on the surface roughness are varied in this study, following the Taguchi method. Their effect is evaluated with respect to the average surface roughness and the maximum surface roughness. The signal-to-noise ratio for the varied parameters infeed, z-pitch, feed rate, and spindle speed is calculated, determining their relevance on the surface roughness, and defining an optimal parameter combination. As the surface quality is optimized to $R_a = 0.47 \mu\text{m}$, the definition of the optimal parameter combination is of the highest relevance for the application of this novel manufacturing approach for Inconel. Using linear regression, the resulting surface roughness of these parameters is predicted, getting validated by the experimental evaluation. Due to a further analysis, including EDX analysis and a quantitative element analysis at different positions of the flank of the milling cutter, wear characteristics as well as the dissipation of the coating of the milling cutter are detected. The flank wear and the resulting breakage of the cutting edge are defined as the main reasons of a rising surface roughness.

Keywords Hybrid laser powder bed fusion · Surface roughness · Taguchi method · High-speed milling · Inconel 718 · EDX analysis

1 Introduction

As the number of industrial applications of laser powder bed fusion (PBF-LB/M) continues to grow, inherent challenges of this technique remain. On the one hand, the advantages of the PBF-LB/M are employed to create new applications, e.g., including complex and lightweight structures [19, 47] as well

as prototypes for aeronautics and aerospace [37], both being inspired by the freedom of design of additive manufacturing and a diverse material selection accessible for PBF-LB/M [23]. On the other hand, still disadvantages are limiting its extended use. Firstly, inferior geometrical accuracy rejects the use for high-precision components [8]. Secondly, the inferior surface quality in comparison to conventional manufacturing technologies necessitates a post-processing [27], for which general 3D-printing aspects such as build orientation [15] and design of support structures [42] as well as the influence of post machining parameters on the mechanical properties have been comprehensively investigated [7, 13, 30]. To promote 3D-production technologies, certain post-processing approaches have been integrated into entire process chains or into single 3D printers to form a hybrid approach, as, e.g., integrating subtractive processes into PBF-LB/M systems [20, 22]. This allows to apply the advantages of additive manufacturing, while eliminating its disadvantages. Popular examples are the combination of, e.g., arc welding to CNC machines, low-cost hybrid techniques have

✉ David Sommer
David.Sommer@th-ab.de

Simon Hornung
s180360@th-ab.de

Cemal Esen
Cemal.Esen@ruhr-uni-bochum.de

Ralf Hellmann
Ralf.Hellmann@th-ab.de

¹ University of Applied Sciences, Applied Laser and Photonics, Würzburger Str. 45, 63743 Aschaffenburg, Germany

² Ruhr University Bochum, Applied Laser Technologies, Universitätsstr. 150, 44801 Bochum, Germany

already been realized industrially [14], and combinations of laser cladding and high-speed milling offer a post-processing 5-axis machining [16, 26, 38]. In this respect, an innovative hybrid approach has recently been designed, as PBF-LB/M and high-speed-milling are combined [29, 36], introducing the powderbed-based additive manufacturing into the hybrid additive manufacturing.

Using this hybrid approach, the geometrical accuracy can be improved, ensuring a fitting accuracy similar to conventional processes [40]. In addition, the surface roughness can significantly be reduced as compared to sole PBF-LB/M, as the surface profile is flattened, as shown by Atabay et al. [2]. While this approach to implement high-speed milling into the PBF-LB/M machine shifts the milling post-processing in situ, it allows to machine contours during the overall build process and thus facilitates to mill inner contours and undercuts, which might be inaccessible after the complete build job [39]. This provides attractive opportunities to foster such applications of PBF-LB/M that demand for superior fitting and surface properties [5].

Among other high-performance metals, Inconel superalloys have also attracted considerable interest in PBF-LB/M applications [10, 18]. While for Inconel machinability in general is challenging [17], the same holds for milling as a post-process for PBF-LB/M [4, 9]. As the integrated high-speed milling process within the hybrid approach studied here represents a unique process, the challenges excel the ones affecting conventional milling, and new knowledge has to be gained to understand and optimize this new manufacturing approach. Due to the powder bed-based process, e.g., no cooling lubricant can be used, raising wear characteristics, reinforcing diffusion, and deteriorating the resulting surface roughness [28, 45]. For this, different parameters of the milling process can be modulated, leading to lower wear characteristics as well as to an increased surface quality.

Against this background, we report on a study about the, novel to Inconel, optimization of surface roughness with a hybrid additive manufacturing approach, combining conventional laser powder bed fusion with a high-speed milling process. As this approach has not been used for a processing of IN718 yet, we specifically study the surface roughness in dependence on different milling parameters, which are systematically varied.

For this purpose, a design of experiment (DoE) is performed, following the Taguchi method to reduce the number of experiments without missing the impact of single parameters. The varied parameters of the integrated high-speed

milling process are feed rate, the performed rotations per minute, the infeed, and the used z-pitch, quantifying the changes with the resulting surface roughness. Using analysis of mean (ANOM) and analysis of variance (ANOVA), the optimal individual parameters and parameter combinations as well as the significance of the parameters are determined. In addition, a linear regression is performed for the prediction of the surface roughness of the optimal parameter combination, getting validated by a final study. Furthermore, the flank wear progress is evaluated, affected by the surrounding powder bed, and the dissipation of coating elements is shown by SEM imaging and EDX analysis.

The results are of utmost importance for a processing of IN718 by this innovative manufacturing approach. Presenting an optimal process window and the achievable surface roughness, this research study paves the way to exploit this novel manufacturing approach for a fabrication of high-performance components.

2 Materials and methods

2.1 Powder properties

In this study, Inconel 718, a nickel superalloy (Heraeus Holding, Hanau, Germany) is processed, exhibiting high strength, good mechanical properties, and corrosion resistance. The used powder material exhibits a particle size distribution between 15 and 45 μm , and the chemical composition is listed in Table 1.

2.2 Machine

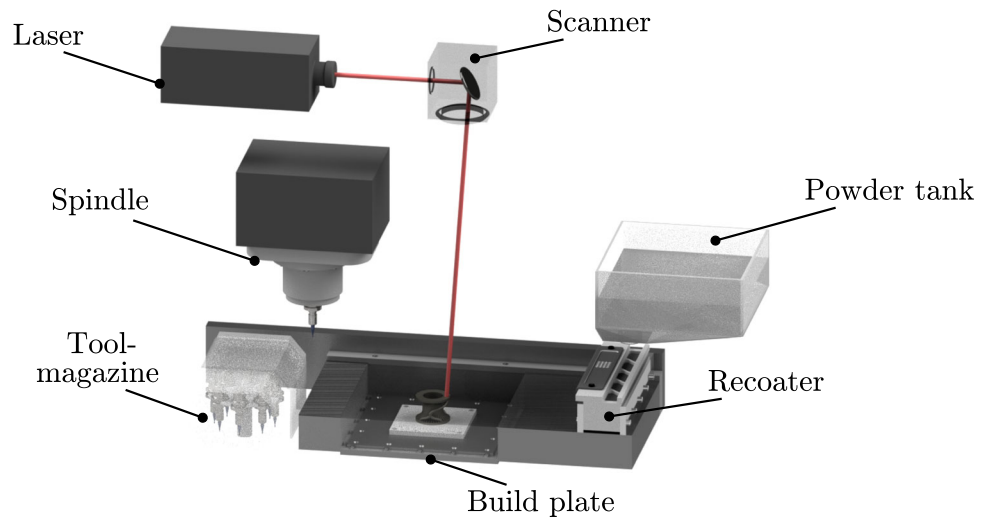
For the hybrid approach, we employed a Lumex Avance-25 (Matsuura Machinery, Wiesbaden, Germany), that combines standard PBF-LB/M and an integrated three-axis milling system, as schematically illustrated in Fig. 1 and depicted in Fig. 2.

For the PBF-LB/M process, the machine is equipped with an ytterbium fibre laser (SPI Lasers, Southampton, UK) with an operating wavelength of 1070 nm and a nominal spot size of 200 μm at focus position. Used PBF-LB/M parameters are summarized in Table 2, the layer height is set to 50 μm , and the maximum build volume is 250 \times 250 \times 185 mm^3 in width, depth, and height. An alternating diagonal scanning

Table 1 Chemical composition of Inconel 718 powder

Element	Ni	Cr	Nb	Mo	Ti	Al	C	Mn	Si	Fe
Wt%	50–55	17–21	4.8–5.5	2.8–3.3	0.7–1.2	0.2–0.8	<0.1	<0.4	<0.4	Balance

Fig. 1 Schematic illustration of the hybrid additive manufacturing unit



strategy is used, using a contour vector for the optimization of the geometrical accuracy. The process is conducted under a nitrogen atmosphere, and the build plate is kept at 50 °C, avoiding thermal stress and deformation.

The high-speed milling process, directly integrated into the PBF-LB/M process, operates with a three-axis high-speed spindle with up to 45,000 rotations per minute and a maximum turning moment of 1.31 Nm. The high-speed milling process does not differ from industrial standard and is equipped with a 20-fold tool magazine, enabling a tool change during operation. The used milling cutters are double-edged solid carbide cutting tools with a cutting radius of 1 mm and a nano-coating, consisting primarily of aluminium and titanium (Mitsubishi Materials Corporation, Meerbusch, Germany). Due to the integration into the PBF-LB/M process, directly machining within the powder bed, no cooling lubricant can be used (Fig. 3). Subsequently, the wear characteristics get reinforced by the dry milling process and the consequentially rising temperature of the milling cutters [34].

For the in situ machining, the PBF-LB/M process is interrupted after ten built layers, with a layer height of 50 µm each. Within the PBF-LB/M, a total material allowance of $a_t = 250 \mu\text{m}$ is added onto the constructed geometry of the components, getting removed gradually by the milling process, as illustrated in Fig. 4a. While the roughing cutter detaches $a_1 = 130 \mu\text{m}$ of the added material in the first step (cf. Fig. 4b), the semi-finishing step removes $a_2 = 90\text{--}110 \mu\text{m}$, preparing the surface texture for the finishing process (cf. Fig. 4c). In a final step, the finishing cutter dissipates the remaining material allowance of $a_3 = 10\text{--}30 \mu\text{m}$, ensuring the best surface quality and superior geometrical accuracy. While the parameters for the finishing process are varied for the optimization of the surface roughness, the adjustments for the roughing as well as for the semi-finishing process are left constant, following Table 3.

The roughing process as well as the semi-finishing step are conducted from the top of the component to the bottom, using a roughing cutter. To avoid residual stress and deformation during the milling process, the finishing cutter starts at lower built layers, moving to the top, sparing the last built layers for the next process cycle (cf. Fig. 4 a and d). Using a customized milling cutter with an increased neck diameter (cf. Fig. 3), a collision is excluded, even though a part of the allowance is spared. Due to this procedure, heat dissipation is optimized, ensuring the best geometrical accuracy and sur-

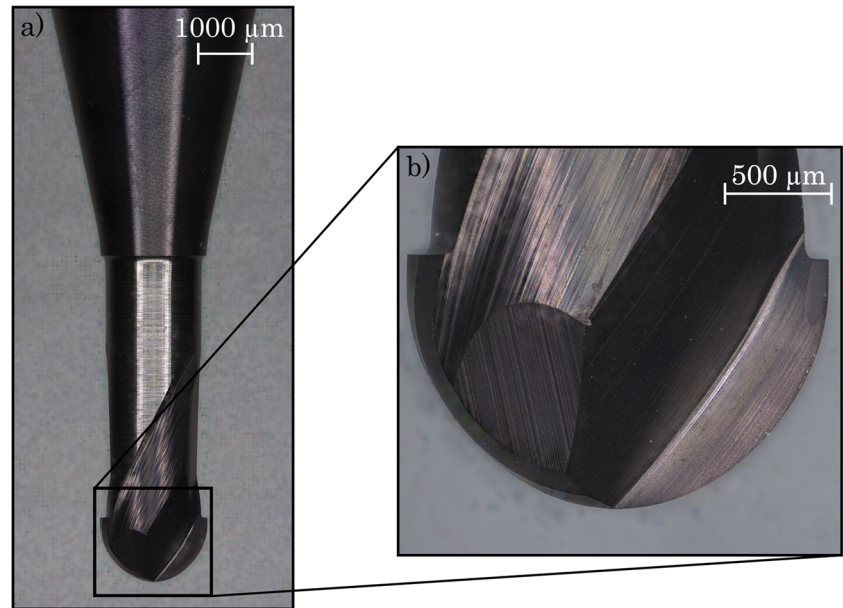


Fig. 2 Hybrid additive manufacturing unit, depicting the recoater, build plate, and the integrated high-speed milling spindle

Table 2 PBF-LB/M parameters

	Laser power (W)	Scan speed (mm/min)	Hatch distance (µm)
Area	320	700	0.12
Contour	320	1400	-
Support	320	700	0.12

Fig. 3 **a** Overview of the finishing cutter and **b** cutting head ($d=2$ mm)



face quality. The PBF-LB/M process generates a heat input, inducing a thermal gradient from the last built layers to the already cooled down parts of the component underneath [3, 31]. Due to the thermal conditions of the PBF-LB/M process, the start of the finishing process at the bottom layers, working upward, is recommended, sparing the last built layers [24, 25].

2.3 Design of experiment

The high-speed milling process is governed by several parameters, influencing the surface roughness directly by virtue of a geometrical impact or indirectly as a process parameter, leading to a difference in the surface roughness by variation [1, 11]. Geometrical milling parameters, varied in this study, are the z-pitch of the milling cutter, directly generating a waviness, and the infeed, defining the load, the milling cutter faces during machining. Milling process parameters, modified for the optimization of the surface roughness, are the feed rate v_f , and the spindle speed n of the milling cutter.

Both can be summarized with the number of cutting edges z quantitatively within the feed per tooth, following Eq. 1:

$$f_z = \frac{v_f}{z * n} \quad (1)$$

As the feed per tooth is, in general, the decisive factor for the high-speed milling process, several studies particularly refer to this. For the micro-milling of Inconel 718, various levels for the feed per tooth are found in literature, optimizing the surface roughness of conventionally or additively manufactured specimens [12, 21, 35, 43].

However, a full factorial study of four parameters with three different levels would lead to $3^4 = 81$ experiments [46]. Using the Taguchi method, a $L_9 (3^4)$ orthogonal array is designed, significantly reducing the number of experiments significantly to nine experiments [44], as shown in Table 4. The used parameters for the optimization of the surface roughness are, as mentioned before, infeed, z-pitch, feed rate, and spindle speed, respectively. The different levels are depicted in Table 5 and lead to a feed per tooth between 4 and $25 \mu\text{m}/\text{tooth}$.

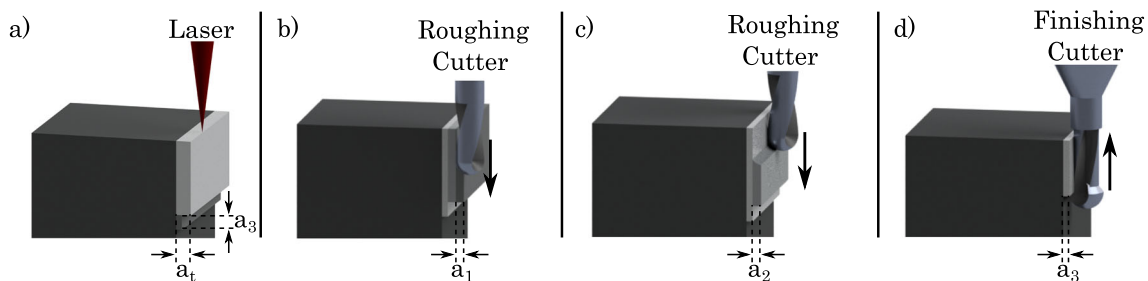


Fig. 4 Process cycle of the hybrid additive manufacturing, integrating an in situ milling process with the **a** PBF-LB/M, **b** roughing, **c** semi-finishing, and **d** finishing process

Table 3 Process parameters for the roughing and semi-finishing process

	Infeed (μm)	Z-pitch (μm)	Spindle speed (rot/min)	Feed rate (mm/min)
Roughing	130	150	4800	240
Semi-finishing	90–110	100	4800	240

The influence of the different parameters is evaluated with the signal-to-noise ratio η (S/N ratio), calculated by the following Eq. 2 with the measured value y and the number of runs for an experiment n , as the surface roughness should be minimized:

$$\eta_i = -10 * \log_{10} \left(\frac{1}{n} * \sum_{i=1}^n y_i^2 \right) \tag{2}$$

In addition, the weighting of the single parameters is calculated, using an ANOM analysis, comparing the means of the different levels of the parameters. The significance is analyzed by an ANOVA approach, pointing out the decisive factors for the optimization of the surface roughness during high-speed milling. According to this, the biggest delta within the different levels of the parameter indicates the statistically most important parameter, while the highest value for the S/N ratio depicts the optimal level for the parameter. As the optimal levels for every parameter are determined, the resulting average surface roughness R_a can be predicted due to linear regression. According to Eq. 3, the coefficients b for the parameters x are calculated, constituting a weighted impact of the parameters on the resulting surface roughness y . A final study can be performed afterwards, applying the optimal parameter combination, validating the statistically predicted value.

$$y = b_0 + b_1 * x_1 + b_2 * x_2 + b_3 * x_3 + b_4 * x_4 \tag{3}$$

Table 4 Orthogonal array for four parameters with three levels each

No.	A	B	C	D
1	1	1	1	1
2	1	2	2	2
3	1	3	3	3
4	2	1	2	3
5	2	2	3	1
6	2	3	1	2
7	3	1	3	2
8	3	2	1	3
9	3	3	2	1

Table 5 Different levels of the varied milling parameters

Parameter	Code	Level 1	Level 2	Level 3
Infeed (μm)	A	30	20	10
Z-pitch (μm)	B	80	100	120
Feed rate (mm/min)	C	240	200	160
Spindle speed (rot/min)	D	4800	9600	19200

2.4 Experimental setup

The experiments are conducted with new milling cutters for every step of the process, excluding any potential effects of tool wear. As test specimens, cubes with 10 mm edge length are fabricated. For every set of parameters, three specimens are built, and the surface roughness of every vertical flank is measured to get a mean for every experiment.

The surface roughness, in detail the average surface roughness R_a and the maximum surface roughness R_z , is measured using a laser scanning microscope (VK-200, Keyence, Osaka, Japan) with a 20× magnification, using an adjustment of inclination to ensure the best results for the measurement. The measurement is conducted, in accordance with ISO 4288 for geometric product specifications—surface textures, above 4.8 mm, and the L-Filter is set to 0.8 mm.

A closer examination of surface textures is obtained with a scanning electron microscope (SEM) (Maia-3, Tescan, Brno, Czech Republic) using the secondary electron detector and a SEM voltage of 5 kV. Further, element analysis is performed with energy-dispersive X-ray spectroscopy, using a VK4 detector (Oxford Instruments, Abingdon, UK) with 15 kV SEM voltage and a beam intensity of 20 pA. The focus of the analysis is set to the elements, utilized for the coating and the shaft, excluding defective signals within the emission spectrum.

3 Results and discussion

The results of the optimization of the surface roughness are summarized in Table 6, revealing an average surface roughness R_a between 0.5 and 0.85 μm (for reference, R_z is provided additionally). Following Eq. 2, the S/N ratio of every observation is determined in relation to R_a , highlighting the influence of the different parameters on the surface roughness.

Apparently, for the optimization of the surface roughness, the infeed is the most important factor, showing the biggest deviation between the different levels, as shown in Table 7. Following the ANOM, the parameter with the largest

Table 6 Process parameters and the resulting surface roughness for the studies

No.	Infeed (μm)	Z-pitch (μm)	Feed rate (mm/min)	Spindle speed (rot/min)	R_a (μm)	R_z (μm)
1	30	80	240	4800	0.69±0.09	5.27±0.47
2	30	100	200	9600	0.78±0.07	6.11±0.61
3	30	120	160	19,200	0.84±0.08	7.12±0.86
4	20	80	200	19,200	0.61±0.04	4.57±0.42
5	20	100	160	4800	0.59±0.07	4.55±0.49
6	20	120	240	9600	0.52±0.07	4.27±0.48
7	10	80	160	9600	0.51±0.05	4.01±0.48
8	10	100	240	19,200	0.61±0.06	4.64±0.42
9	10	120	200	4800	0.57±0.10	4.26±0.60

delta represents the biggest impact on the resulting value. As shown in the main effect plot for S/N ratios in Fig. 5, the best level for the infeed is $a_3 = 10 \mu\text{m}$ with a S/N ratio of 4.990, while the infeed of $a_3 = 30 \mu\text{m}$ shows a S/N ratio of 2.319, getting validated by $p \leq \alpha$. However, as the infeed defines the load, the milling cutter faces during processing, a smaller infeed provides a lower impact on the milling cutter, leading to slighter tool wear and superior surface roughness. At the manufacturing of IN718, the infeed directly affects the flank wear, whereby it is clarified as a determinant for the generation of a good surface quality [6].

As the second most important parameter, the spindle speed is defined with a delta of 1.201 between the different levels. It turns out that 9600 rot/min is an optimal value for the optimization of the surface roughness. Due to the higher load at minor rotational velocities, the flank of the milling cutter cracks, directly affecting the quality of the finished surface. At higher rotations, the coating of the milling cutter gets burned in consequence of the rising temperature development, leading to an inferior performance as well. As the flank of the milling cutter, especially the finishing cutter, depicts a critical point within the milling process, the spindle speed must be selected well. Unadjusted parameters lead to higher wear characteristics, affecting the resulting surface quality negatively, as a new cutting edge is formed by the abrasion [43].

As mentioned before, the z-pitch directly generates a waviness at the surface profile, minimizing with smaller z-pitches. With that, the optimal surface roughness develops at a z-pitch of $80 \mu\text{m}$ with a S/N ratio of 4.497. Following this,

Table 7 S/N ratio of the varied milling parameters

Level	Infeed	Z-pitch	Feed rate	Spindle speed
1	4.990	4.497	4.013	4.211
2	4.834	3.636	3.754	4.567
3	2.319	4.009	4.376	3.365
Delta	2.671	0.861	0.623	1.201
Rank	1	3	4	2

the z-pitch can be further reduced for the minimization of the surface roughness marginally, yet in turn increasing the manufacturing time.

Finally, the feed rate provokes the smallest impact on the surface quality, getting optimal results at $v_f = 240 \text{ mm/min}$. As shown in Eq. 1, combined with the spindle speed, the feed rate defines the feed per tooth f_z as a decisive factor. In this respect, the impact of the feed rate can be diminished by the elevated importance of the spindle speed, both leading to the same quantitative result in interaction [41]. At the application of milling technologies, a compromise must be found for those two parameters for the best combination.

Flank wear is generally considered a measurable indicator of tool wear, reported before by several studies [11, 32, 33]. Figure 6 shows one flank of the finishing cutter for every experiment after about 120 min of operation. The extent of the flank wear is compared, occurring by virtue of the different parameter combinations of the studies. Apparently, the flank of all finishing cutters shows wear mechanisms, leading to an abrasion of the coating as well as to a cobbling of the solid carbide underneath for some cutters. Due to different wear mechanisms, the coating of the flank gets dissipated, causing flank wear in various peculiarities. For higher rotational velocities combined with a high feed rate, diffusion reinforces wear characteristics in consequence of the elevating temperature (cf. No. 3 and No. 4). At lower rotational velocities with an unadjusted feed rate, the mechanical load exceeds the mechanical resistance of the milling cutter, resulting in disruptions of the flank wear (cf. No. 1 and No. 9) [11].

Figure 7 summarizes the SEM analysis of the milling cutter, detailing the effects of the flank wear, the removal of the coating, comparing these with an unused milling cutter. The unused milling cutter shows the coating, consisting primarily of titanium and aluminium nitrate, as further elements are not depicted for a well-arranged depiction. Please note that the milling cutters get grinded after coating for an increased neck diameter, required for the finishing process. Thus, the coating of the unused milling cutter is removed at the edge of the

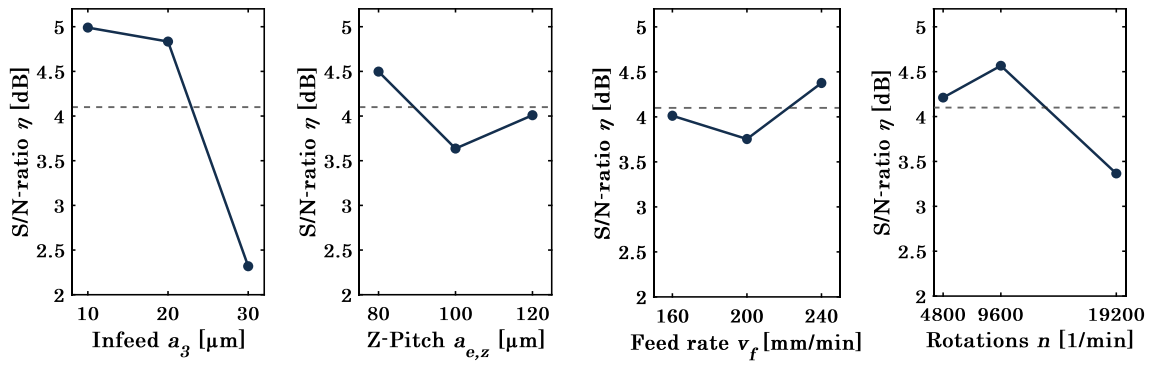


Fig. 5 Main effect plots for the analysis of the S/N ratio of the different process parameters

neck, showing the base material, comprised out of tungsten carbide (cf. Fig. 7a).

At the used milling cutter of study No. 8 (cf. Fig. 7b), the coating is removed partly at the edge of the flank, getting dissipated by the common wear characteristics and the elevating temperature, resulting out of a high spindle speed. The remaining flank is still coated, and a further flank wear is acceptable, still expecting a good surface quality.

In turn, the flank of the milling cutter, used in study No. 9, is worn, a part of the flank is busted, and the coating is, obviously, removed (cf. Fig. 7c). By virtue of the low spindle speed and the incidental higher load for the milling cutter, the flank wear increases, leading to a breakout, as shown in detail in Fig. 7 d, e, and f. As depicted in the EDX mapping, worn parts of the flank only show tungsten and carbon, excluding the elements of the coating at this position. Quantitative element analysis shows the characteristic peaks for

tungsten and carbide, detecting only a weak signal for the coating elements. Tungsten, used as a backing material due to its hardness, predominates the spectral analysis (cf. Fig. 7g), proving a complete removal of the coating, evidently caused by the breakout.

At point 2, labelled in Fig. 7e, the coating still exists and is not dissipated by the flank wear. The spectrum for the element analysis is partitioned between the different coating elements, primarily showing peaks for aluminium and nitrogen, getting completed by titanium and chromium as well as by nickel and traces of iron and niobium (cf. Figure 7 h).

The best milling parameters, transpired out of the optimization of the surface roughness, are $a_3 = 10\mu\text{m}$ for the infeed, a z-pitch of $a_{e,z} = 80\mu\text{m}$, a feed rate of $v_f = 240\text{ mm/min}$, and $n = 9600\text{ rot/min}$ for the spindle speed (cf. Table 8). According to Eq. 3, the resulting average surface roughness can be predicted, using the calculated coefficients.

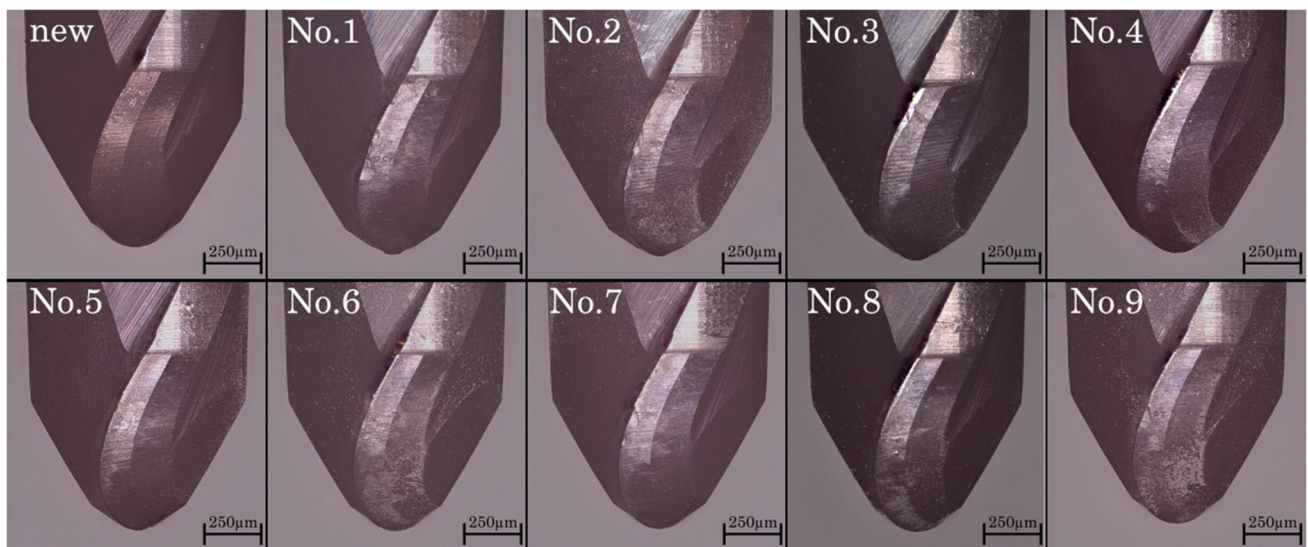


Fig. 6 Flank wear analysis for the finishing cutters

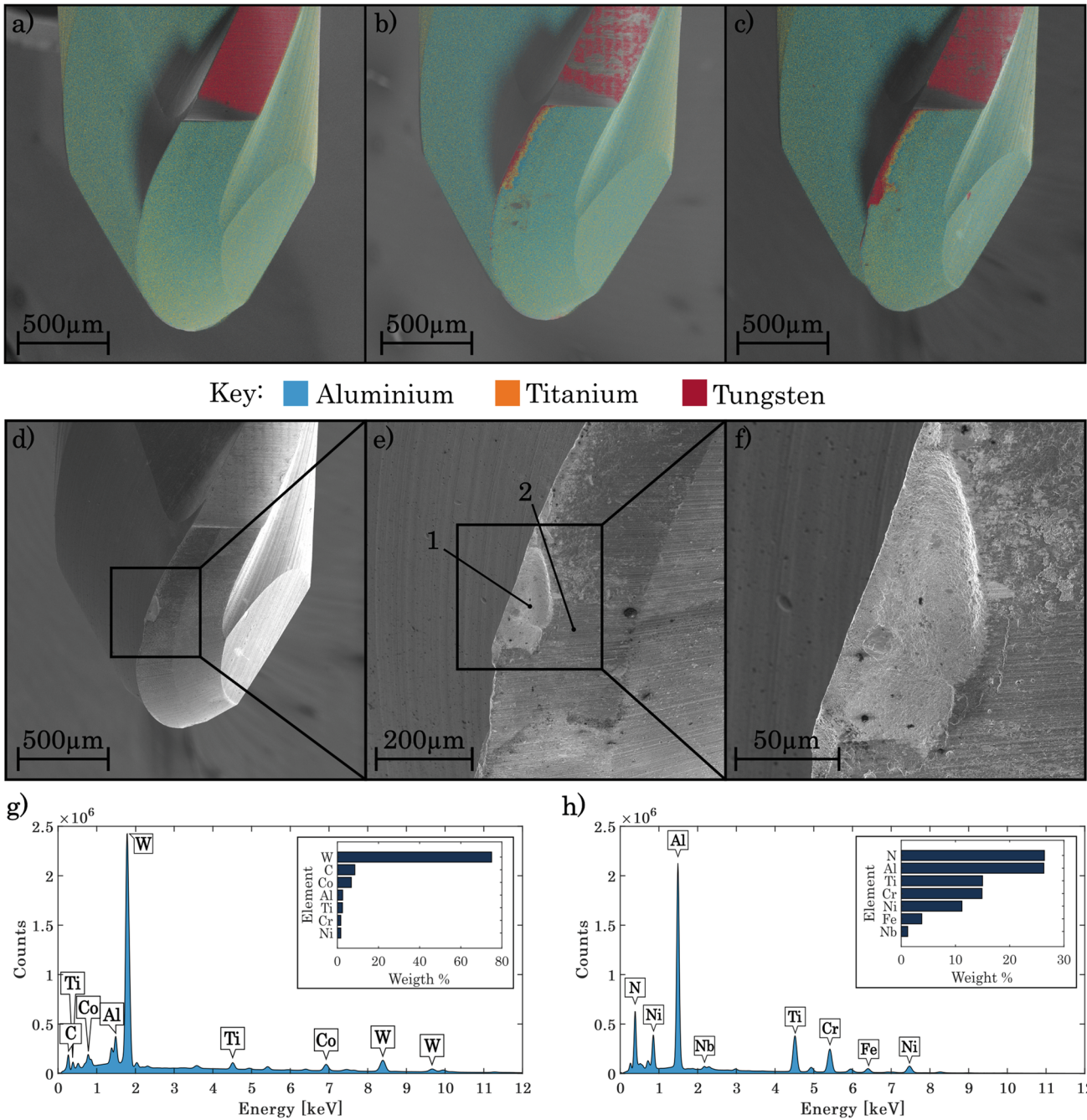


Fig. 7 SEM images with a distribution of elements of **a** new finishing cutter, **b** finishing cutter No. 8, **c** finishing cutter No. 9, **d–f** SEM images of the outbreak of the finishing cutter No. 9, and element spectrum for **g** outbreak (point 1) and **h** coating (point 2)

Following Eq. 4, the average surface roughness results to $R_a = 0.5045 \mu\text{m}$.

$$R_a = 0.356 + 0.01017 * a_3 + 0.00108 * a_{e,z} - 0.000455 * v_f + 0.000005 * n \quad (4)$$

To validate this prediction, the derived optimized parameter combination, as summarized in Table 8, is employed in

a further print and milling process. The resulting specimen exhibits a surface roughness of $R_a = 0.47 \mu\text{m}$ and excels the

Table 8 Optimized process parameters for the finishing process

	Infeed (μm)	Z-pitch (μm)	Feed rate (mm/min)	Spindle speed (rot/min)
Finishing process	10	80	240	9600

predicted optimized value slightly. For the maximum surface roughness, a value of $R_z = 3.73 \mu\text{m}$ is investigated, depicting the minimum for the study as well.

4 Conclusion

Within this study, the surface roughness of hybrid additive manufactured Ni superalloy was optimized. Using an in situ milling process and the difficult-to-machine material IN718, challenges of this innovative approach have to be mastered, resulting in an advanced surface quality for 3D-built components. Compared to maraging steel, concerned in previous studies, the machining of IN718 faces increased wear characteristics, necessitating a detailed study of the process parameters.

Based on the Taguchi method, the relevant influencing parameters on the milling process were varied. As a result, a set of optimized milling parameters is determined that leads to a superior surface roughness of $R_a = 0.47 \mu\text{m}$ and $R_z = 3.73 \mu\text{m}$. Using linear regression, the achievable surface roughness could be predicted to $R_a = 0.50 \mu\text{m}$. In comparison to sole PBF-LB/M-built components, the surface roughness is lowered significantly, leading to superior geometrical accuracy and suitability for industrial applications with strict tolerances.

Furthermore, the flank wear was analyzed for every parameter combination, revealing different wear characteristics, caused by, e.g., low spindle speed and subsequently high rising load for the milling cutter. As the flank of the milling cutter gets worn, an EDX analysis was used to qualify the dissipation of the coating and the subsequent reveal of the backing material.

Within the following research, a closer examination of changes in microstructure can be done, qualifying the impact of the subsequent machining process for the Ni superalloy. Furthermore, the usage of different materials like, e.g., Ti and Al alloys can be interesting, as the wear characteristics and the resulting surface quality can be fundamentally different.

Author contribution All authors contributed to the study conception and design. All authors read and approved the final manuscript.

Funding Open Access funding enabled and organized by Projekt DEAL.

Declarations

Conflict of interest The authors declare no competing interests.

Open Access This article is licensed under a Creative Commons Attribution 4.0 International License, which permits use, sharing, adaptation, distribution and reproduction in any medium or format, as long as you give appropriate credit to the original author(s) and the

source, provide a link to the Creative Commons licence, and indicate if changes were made. The images or other third party material in this article are included in the article's Creative Commons licence, unless indicated otherwise in a credit line to the material. If material is not included in the article's Creative Commons licence and your intended use is not permitted by statutory regulation or exceeds the permitted use, you will need to obtain permission directly from the copyright holder. To view a copy of this licence, visit <http://creativecommons.org/licenses/by/4.0/>.

References

- Aslantas K, Alatrushi LKH (2021) Experimental study on the effect of cutting tool geometry in micro-milling of Inconel 718. *Arab J Sci Eng* 46(3):2327–2342. <https://doi.org/10.1007/s13369-020-05034-z>
- Atabay SE, Wanjara P, Bernier F et al (2022) In envelope additive/subtractive manufacturing and thermal post-processing of Inconel 718. *Materials* 16(1). <https://doi.org/10.3390/ma16010001>
- Cheng B, Shrestha S, Chou K (2016) Stress and deformation evaluations of scanning strategy effect in selective laser melting. *Addit Manuf* 12:240–251. <https://doi.org/10.1016/j.addma.2016.05.007>
- Danish M, Aslantas K, Hascelik A et al (2022) An experimental investigations on effects of cooling/lubrication conditions in micro milling of additively manufactured Inconel 718. *Tribol Int* 173:107620. <https://doi.org/10.1016/j.triboint.2022.107620>, <https://www.sciencedirect.com/science/article/pii/S0301679X22001931>
- Dilberoglu UM, Gharehpapagh B, Yaman U et al (2021) Current trends and research opportunities in hybrid additive manufacturing. *Int J Adv Manuf Technol* 113(3–4):623–648. <https://doi.org/10.1007/s00170-021-06688-1>
- Dudzinski D, Devillez A, Moufki A et al (2004) A review of developments towards dry and high speed machining of Inconel 718 alloy. *Int J Mach Tools Manuf* 44(4):439–456. [https://doi.org/10.1016/S0890-6955\(03\)00159-7](https://doi.org/10.1016/S0890-6955(03)00159-7), <https://www.sciencedirect.com/science/article/pii/S0890695503001597>
- Fei J, Liu G, Patel K et al (2020) Effects of machining parameters on finishing additively manufactured nickel-based alloy Inconel 625. *J Manuf Mater Process* 4(2):32. <https://doi.org/10.3390/jmmp4020032>, <https://www.mdpi.com/2504-4494/4/2/32>
- Giganto S, Martínez-Pellitero S, Cuesta E et al (2022) Proposal of design rules for improving the accuracy of selective laser melting (SLM) manufacturing using benchmarks parts. *Rapid Prototyp J*. <https://doi.org/10.1108/RPJ-06-2021-0130>
- Halim N, Haron C, Ghani JA et al (2019) Tool wear and chip morphology in high-speed milling of hardened Inconel 718 under dry and cryogenic CO2 conditions. *Wear* 426–427:1683–1690. <https://doi.org/10.1016/j.wear.2019.01.095>, <https://www.sciencedirect.com/science/article/pii/S0043164819302698>
- Hwang JR, Zheng JY, Kuo PC et al (2022) Process optimization of Inconel 718 alloy produced by laser powder bed fusion. *Metals* 12(9):1494. <https://doi.org/10.3390/met12091494>, <https://www.mdpi.com/2075-4701/12/9/1494>
- Ji H, Gupta MK, Song Q et al (2021) Microstructure and machinability evaluation in micro milling of selective laser melted Inconel 718 alloy. *J Mater Res Technol* 14:348–362. <https://doi.org/10.1016/j.jmrt.2021.06.081>, <https://www.sciencedirect.com/science/article/pii/S2238785421006360>
- Jia Z, Lu X, Gu H et al (2021) Deflection prediction of micro-milling Inconel 718 thin-walled parts. *J Mater Process Technol* 291:117003. <https://doi.org/10.1016/j.jmatprotec.2020.117003>, <https://www.sciencedirect.com/science/article/pii/S0924013620304258>

42. Tripathi V, Armstrong A, Gong X et al (2018) Milling of Inconel 718 block supports fabricated using laser powder bed fusion. *J Manuf Process* 34:740–749. <https://doi.org/10.1016/j.jmapro.2018.03.046>, <https://www.sciencedirect.com/science/article/pii/S1526612518305772>
43. Ucun İ, Aslantas K, Bedir F (2013) An experimental investigation of the effect of coating material on tool wear in micro milling of Inconel 718 super alloy. *Wear* 300(1–2):8–19. <https://doi.org/10.1016/j.wear.2013.01.103>, <https://www.sciencedirect.com/science/article/pii/S0043164813001257>
44. Unal R, Dean EB (1991) Taguchi approach to design optimization for quality and cost: an overview. *Annual Conference of the International Society of Parametric Analysts*. <https://ntrs.nasa.gov/citations/20040121019>
45. Yin Q, Liu Z, Wang B et al (2020) Recent progress of machinability and surface integrity for mechanical machining Inconel 718: a review. *Int J Adv Manuf Technol* 109(1–2):215–245. <https://doi.org/10.1007/s00170-020-05665-4>
46. Zhang JZ, Chen JC, Kirby ED (2007) Surface roughness optimization in an end-milling operation using the Taguchi design method. *J Mater Process Technol* 184(1–3):233–239. <https://doi.org/10.1016/j.jmatprotec.2006.11.029>, <https://www.sciencedirect.com/science/article/pii/S0924013606009393>
47. Zhonghua L, Zhengwen Zhang D, Dong P et al (2017) A lightweight and support-free design method for selective laser melting. *Int J Adv Manuf Technol* 90(9):2943–2953. <https://doi.org/10.1007/s00170-016-9509-0>

Publisher's Note Springer Nature remains neutral with regard to jurisdictional claims in published maps and institutional affiliations.